npj computational materials

www.nature.com/npjcompumats

ARTICLE OPEN

Check for updates

Circumventing the phonon bottleneck by multiphonon-mediated hot exciton cooling at the nanoscale

Dipti Jasrasaria[1,4]✉ and Eran Rabani[1,2,3]✉

Nonradiative processes govern efficiencies of semiconductor nanocrystal (NC)-based devices. A central process is hot exciton cooling, or the nonradiative relaxation of a highly excited electron/hole pair to form a band-edge exciton. Due to quantum confinement effects, the timescale and mechanism of cooling are not well understood. A mismatch between electronic energy gaps and phonon frequencies has led to the hypothesis of a phonon bottleneck and extremely slow cooling, while enhanced electron-hole interactions have suggested ultrafast cooling. Experimental measurements of the cooling timescale range six orders of magnitude. Here, we develop an atomistic approach to describe phonon-mediated exciton dynamics and simulate cooling in NCs of experimentally relevant sizes. We find that cooling occurs on ~30 fs timescales in CdSe NCs, in agreement with the most recent measurements, and that the phonon bottleneck is circumvented through a cascade of multiphonon-mediated relaxation events. Furthermore, we identify NC handles for tuning the cooling timescale.

npj Computational Materials (2023)9:145 ; https://doi.org/10.1038/s41524-023-01102-8

INTRODUCTION

Understanding mechanisms of nonradiative decay of electronic excited states in semiconductor nanocrystals (NCs) is key to developing NC-based technologies with decreased thermal losses and increased device efficiencies[1–6]. When a NC is excited by a photon with an energy larger than that of the NC band gap, the absorbed photon generates a highly excited electron-hole pair. The process by which these excited, or "hot", carriers nonradiatively relax to form a band edge exciton is often referred to as "hot exciton cooling[7,8]." In bulk semiconductors, Fröhlich and deformation potential interactions between excitons and phonons, as well as continuous densities of electronic and phonon states, allow for efficient hot exciton cooling that occurs on timescales of ~1 ps or less[9–11]. However, in semiconductor NCs, confinement changes the nature of exciton-phonon coupling (EXPC) and leads to the discretization of both electronic and phonon states. These qualitative changes have led to open questions regarding the timescales and mechanisms of hot exciton cooling in confined semiconductor materials[7,8,12,13].

In a picture of noninteracting electrons and holes, the hot electron and hot hole would relax independently from one another. The hole, which has a heavier effective mass than the electron in most II-VI and III-V semiconductors, has a higher density of states with energy gaps that are on the order of the phonon frequencies in the system[14]. Thus, resonance conditions required for hole relaxation *via* single-phonon emission can be easily satisfied, and the hole can relax quickly to the band edge. The electron, however, has energy gaps, especially near the conduction band edge, that can be hundreds of meV, which is an order of magnitude larger than the typical optical phonon frequencies in the system[14]. This energy mismatch has led to the hypothesis of a phonon bottleneck in NCs[15], where hot electron cooling *via* phonon emission would require a multiphonon process, as depicted in Fig. 1a. The simultaneous emission of tens of phonons would be inefficient[16], leading to very slow relaxation.

Experimental measurements of this cooling process in NCs rely on time-resolved spectroscopy, such as transient absorption, and have yielded conflicting results. Some experiments show slow relaxation that occurs on timescales of 10 ps or longer[17–23], which supports the phonon bottleneck hypothesis. These measurements were primarily performed on larger, self-assembled III-V NCs[24], which are in the weak confinement regime and which tend to have many localized trap states associated with structural defects. Other experiments, especially on colloidal II-VI NCs in the strong confinement regime, have observed relaxation that occurs within hundreds of femtoseconds with carrier energy loss rates that are much faster than those of bulk carriers[25–31].

This fast relaxation of strongly confined electron-hole pairs was attributed to an Auger-assisted cooling mechanism that circumvents the phonon bottleneck through Coulomb-mediated interactions between the electron and hole[32,33]. In this mechanism, illustrated schematically in Fig. 1b, the hot hole quickly relaxes to the band edge *via* phonon emission. Then, the hot electron relaxes to the band edge by nonradiatively re-exciting the hole in an Auger-like process, and finally, the hole relaxes again. The Auger cooling mechanism has been supported by observations that relaxation is faster in smaller NCs[25,26,28,30,34], in which electron-hole correlations are larger and Auger rates are faster[35]. Additionally, relaxation timescales increase drastically in NCs that are passivated with hole-accepting pyridine ligands[20,27,36], indicating that electron-hole correlations are important in the cooling mechanism. Other studies suggest that fast relaxation is due to efficient multiphonon emission[28] or due to the coupling of electrons and/or holes to the vibrational modes of surface passivating ligands[31,36].

While the Auger cooling mechanism provides an avenue for breaking the phonon bottleneck, it lacks essential physics for a complete description of hot exciton cooling in NCs. For example,

[1]Department of Chemistry, University of California, Berkeley, CA 94720, USA. [2]Materials Sciences Division, Lawrence Berkeley National Laboratory, Berkeley, CA 94720, USA. [3]The Sackler Center for Computational Molecular and Materials Science, Tel Aviv University, Tel Aviv 69978, Israel. [4]Present address: Department of Chemistry, Columbia University, New York, NY 10027, USA. ✉email: djasrasaria@berkeley.edu; eran.rabani@berkeley.edu

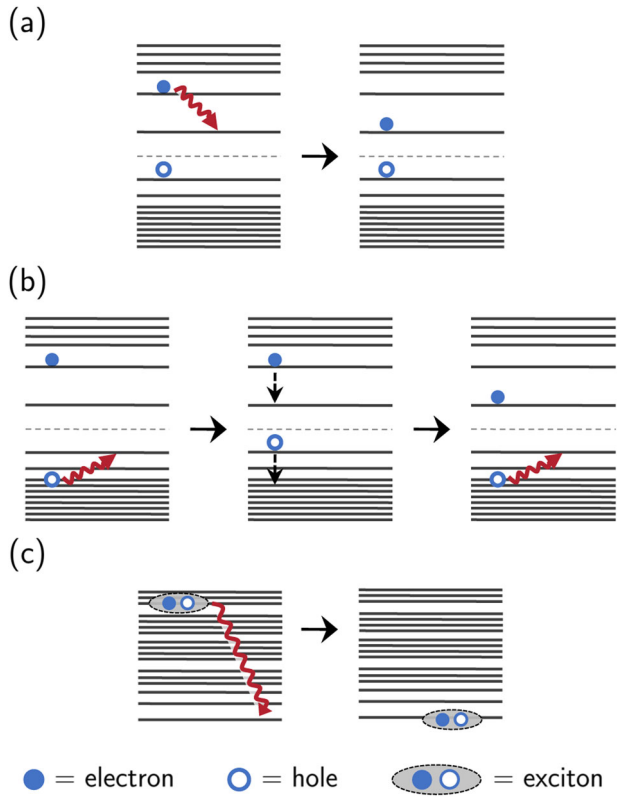

Fig. 1 Proposed mechanisms of hot exciton cooling. a The phonon bottleneck refers to phonon-mediated, hot electron relaxation near the band edge, which would require the simultaneous emission of several of phonons due to the large energy gaps between these single-particle electronic states. **b** The Auger-assisted cooling mechanism involves Coulomb-mediated interactions between electron and hole states. The hole first relaxes to the band edge *via* phonon emission. Then, the electron relaxes by re-exciting the hole, which then relaxes to the band edge once more. **c** Our formalism includes both electron-hole correlations and exciton-phonon interactions, circumventing the phonon bottleneck through a cascade of phonon-mediated transitions between *excitonic* states with smaller energy gaps.

electron-hole interactions, which are enhanced in confined semiconductors[14], are only considered perturbatively. Furthermore, the Auger cooling mechanism lacks the mechanistic details of the rapid hole relaxation and, for certain systems[31,37], may result in a hole phonon bottleneck when multiphonon relaxation pathways are assumed to be negligible.

The computational challenges[38–44] associated with accurately calculating excitons and their phonon-mediated dynamics in systems with thousands of valence electrons and hundreds of atoms have made it difficult to delineate the mechanism of hot exciton cooling and its dependence on NC properties, such as size and material composition[7,8]. A fundamental understanding of this process may offer rational design principles for NCs with tuned cooling timescales that are optimized for different NC-based applications[4,12,23,45].

Here, we develop an atomistic theory to describe hot exciton cooling in II-VI NCs of experimentally relevant sizes. Our framework describes phonon-mediated transitions between *excitonic* states, which inherently include electron-hole correlations (Fig. 1c). Furthermore, we accurately describe the exciton-phonon couplings (EXPC)[46,47] and include multiphonon-mediated excitonic transitions. We use a master equation approach, which assumes weak EXPC, to propagate exciton population dynamics.

The timescales and exciton decay mechanism emerge naturally in our approach. We find that cooling occurs on timescales of tens of femtoseconds in wurtzite CdSe NCs, in agreement with measurements[26,30], and occurs an order of magnitude slower in wurtzite CdSe-CdS core-shell NCs due to the weaker EXPC in these systems. We show that this ultrafast timescale is governed by *both* electron-hole correlations *and* multiphonon emission processes, which are made efficient by the quasi-continuous manifold of phonon states in NCs. Our results are consistent with the picture emerging from the Auger-assisted relaxation mechanism, but, in addition, we attribute the lack of a phonon bottleneck to the important role of multiphonon emission processes.

RESULTS AND DISCUSSION

Describing phonon-mediated exciton cooling

We adopt the following Hamiltonian to describe a manifold of excitonic states coupled to vibrational modes, with EXPC expanded to the lowest order in the atomic displacements:[46]

$$H = \sum_n E_n |\psi_n\rangle\langle\psi_n| + \sum_\alpha \hbar\omega_\alpha b_\alpha^\dagger b_\alpha + \sum_{\alpha nm} V_{n,m}^\alpha |\psi_n\rangle\langle\psi_m| q_\alpha \,. \quad (1)$$

The excitonic energies, E_n, and states, $|\psi_n\rangle$, as well as the EXPC matrix elements, $V_{n,m}^\alpha$, were calculated using the semiempirical pseudopotential method coupled with the Bethe-Salpeter equation (see Jasrasaria et al.[14,46] and the SI for more details). Phonon modes and frequencies, ω_α, were obtained by diagonalizing the dynamical matrix computed using a previously-parameterized atomic force field[48].

In Fig. 2a we show the density of excitonic states scaled by the oscillator strengths for a typical CdSe NC with a diameter of 3.9 nm, as well as the corresponding linear absorption spectrum. We find that the underlying density of excitonic states is relatively high due to the dense spectrum of hole states. Some of these excitonic states correspond to *bright* transitions from the ground state with large oscillator strengths, while others correspond to *dim* transitions for which the oscillator strengths are small. Note that we only show the bright/dim states, and the dark (spin-forbidden) transitions are not shown. The linear absorption spectrum shows several distinct features, in agreement with experiments[26,49], that are governed by a few excitonic transitions with large oscillator strengths. We label the main transitions as 1*S* and 1*P*, following the literature convention. With the dense manifold of excitonic states, the relaxation from the 1*P* excitonic state, in which the exciton electron is primarily composed of *p*-like, single-particle electron states, to the 1*S* ground excitonic state, in which both the exciton electron and hole are primarily comprised of band edge single-particle states, should occur through a cascade of phonon-mediated transitions, where both bright and dim excitonic states are involved.

We first consider the limit of single-phonon processes. We adopt the Redfield equation[50] and propagate the reduced density matrix, which describes the subspace of excitons, using a quantum master equation that is perturbative to second order in the EXPC, as the EXPC is weak compared to other energy scales in the NCs studied here. The dynamics of the exciton populations and coherences are coupled very weakly in these systems, and thus we only model the population dynamics. In this limit, the Redfield equation reduces to a kinetic master equation for the populations, where the transition rates are given by the time-dependent golden rule rates. The phonon-mediated transition rate between excitonic states n and m is given by

$$\Gamma_{n\to m}(t) = \frac{1}{\hbar^2}\int_{-t}^{t} d\tau e^{i(E_n - E_m)\tau/\hbar} \sum_\alpha V_{n,m}^\alpha V_{m,n}^\alpha \langle q_\alpha(\tau) q_\alpha(0)\rangle_{\text{eq}} \,, \quad (2)$$

where $\langle \dots \rangle_{\text{eq}}$ denotes an equilibrium average over bath coordinates. We computed these rates for all excitonic transitions

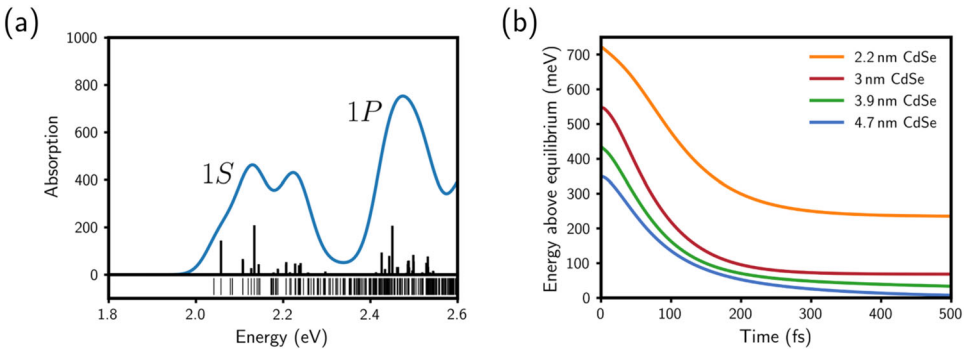

Fig. 2 Single-phonon-mediated hot exciton cooling. a The calculated linear absorption spectrum (top) and density of excitonic states (bottom) for a 3.9 nm CdSe NC. The vertical lines in the top panel indicate the magnitude of the oscillator strength of the transition from the ground state to that excitonic state. Cooling from the 1*P* to the 1*S* excitonic states, whose transitions are labeled in the absorption spectrum, is the main subject of this work. **b** Single-phonon-mediated hot exciton cooling simulated for CdSe NCs of different sizes shows a phonon bottleneck in smaller NCs because excitonic energy gaps in those systems are larger than the highest phonon frequencies.

and used them to build a kinetic master equation and propagate phonon-mediated exciton dynamics:

$$\dot{p}_n(t) = \sum_{m\neq n}\left(\Gamma_{m\to n}(t)p_m(t) - \Gamma_{n\to m}(t)p_n(t)\right), \tag{3}$$

where $p_n(t)$ is the population of state n at time t. We then calculated the average energy above equilibrium, $\langle \Delta E(t)\rangle = \sum_n E_n\left(p_n(t) - p_{n,\mathrm{eq}}\right)$, where $p_{n,\mathrm{eq}} = e^{-\beta E_n}/\left(\sum_m e^{-\beta E_m}\right)$ is the population of state n at thermal equilibrium and $\beta = (k_B T)^{-1}$.

Because Eq. (1) describes the EXPC to first order in the phonon mode coordinates, the golden rule rates given by Eq. (2) only account for excitonic transitions that occur *via* the absorption or emission of a single phonon. While the largest energy gaps between excitonic states are an order of magnitude smaller than those between single-particle electron states, they can still be larger than the phonon frequencies. Thus, transitions between those excitonic states would require the simultaneous emission of multiple phonons. Indeed, single-phonon-mediated cooling simulations for CdSe NCs of different sizes show a phonon bottleneck in NCs smaller than 4.7 nm in diameter (Fig. 2b). This phonon bottleneck is especially significant in smaller NCs for which confinement results in larger excitonic energy gaps, particularly at low excitonic energies, preventing the hot exciton from fully relaxing to the band edge through single-phonon emission.

Multiphonon emission

To account for multiphonon processes and maintain the simplicity of the master equation, we performed a unitary polaron transformation[51–54] to the Hamiltonian in Eq. (1):

$$\tilde{H} = e^{S} H e^{-S}, \tag{4}$$

where

$$S = -\frac{i}{\hbar}\sum_{ak}\omega_a^{-2} p_a V^a_{k,k}|\psi_k\rangle\langle\psi_k|, \tag{5}$$

and p_a is the momentum of phonon mode a. A detailed derivation and description of the polaron-transformed Hamiltonian and its consequences are given in the Supplementary Information.

With respect to the polaron-transformed Hamiltonian, golden rule transition rates can be computed as

$$\Gamma_{n\to m}(t) = \frac{1}{\hbar^2}\int_{-t}^{t} d\tau e^{i(\varepsilon_n-\varepsilon_m)\tau/\hbar}\langle g_{n,m}(\tau)g_{m,n}(0)\rangle_{\mathrm{eq}}, \tag{6}$$

where $\varepsilon_n \equiv E_n - \lambda_n$ is the energy of exciton n scaled by its reorganization energy, and $g_{n,m} \equiv \sum_a \tilde{V}^a_{n,m} q_a - \tilde{\lambda}_{nm}$ is the coupling between the polaronic states n and m (see the SI for more details). Again, we computed all transition rates to build a kinetic master equation and propagate dynamics. Within this framework, we calculate the average energy above thermal equilibrium as before; namely, as $\langle \Delta\varepsilon(t)\rangle = \sum_n \varepsilon_n\left(p_n(t) - p_{n,\mathrm{eq}}\right)$.

Note that $g_{n,m}$ includes exponential functions of the phonon momenta, so multiphonon-mediated transitions are accounted for even in the lowest order perturbation theory rate given by Eq. (6). Including multiphonon processes enables transitions between excitonic states that have energy differences that are larger than the highest-frequency phonons. Multiphonon-mediated cooling simulations show that all NC systems fully relax to thermal equilibrium (Fig. 3a), indicating that multiphonon transitions involving a few phonon modes are essential to the cooling mechanism. Furthermore, the average energy relaxes within 100 fs, much faster within the single-phonon scheme. The simulated average energy normalized to the energy of the thermal equilibrium state for each CdSe NC is illustrated in Supplementary Fig. 2.

Examining the transition rate as a function of transition energy for a 3.9 nm CdSe NC, illustrated in Fig. 3b, demonstrates that the single-phonon rates are larger for low-energy transitions, but there are no single-phonon transitions between excitonic states that have energy differences greater than ~32 meV (i.e., greater than the largest phonon energy). The multiphonon rates, however, cover the full range of transition energies. Importantly, multiphonon relaxation between excitonic states with energy differences of 100 meV or less consistently have relatively high rates (ranging from $10^{-3} - 10^{2}$ ps^{-1} for multiphonon transitions as compared to $0-10^{2}$ ps^{-1} for single-phonon transitions). This difference makes accessible many more relaxation channels and leads to a cooling timescale that is an order of magnitude faster than that resulting from single-phonon processes alone. The fast multiphonon relaxation is a result of the large number of phonon modes (approximately 3000 modes for a 3.9 nm CdSe NC) that quasi-continuously span a wide frequency range and that are all coupled, to some degree, to excitonic transitions. Thus, many phonon combinations satisfy the energy conservation requirement for phonon-mediated exciton transitions, leading to efficient relaxation *via* the emission of multiple phonons.

The asymmetry in rates about 0 meV transition energy reflects detailed balance (see Methods for more details). Furthermore, Fig. 3b shows a Gaussian relationship between the transition energy and the transition rate instead of the exponential dependence of the rate on the energy that results from the assumption that only the highest-frequency modes participate in nonradiative transitions[55]. This result indicates that lower-frequency acoustic *and* optical modes are important to this cooling process, extending

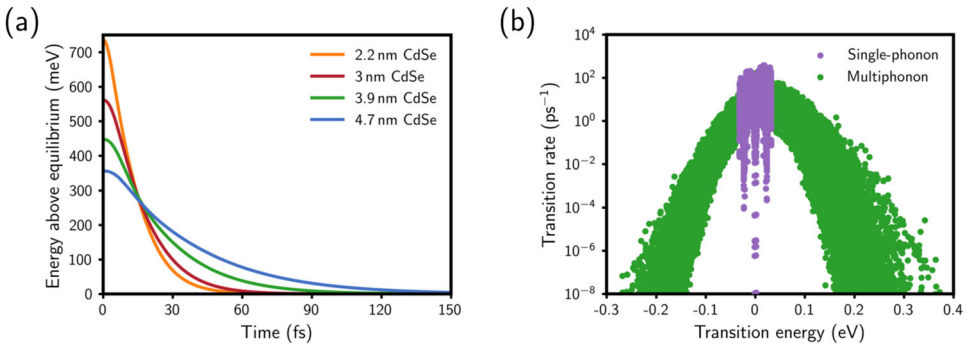

Fig. 3 Multiphonon-mediated hot exciton cooling. a Hot exciton cooling simulated for CdSe cores of different sizes. The inclusion of multiphonon processes allows all systems to relax to thermal equilibrium, eliminating the phonon bottleneck. **b** Exciton transition rates calculated for a 3.9 nm CdSe NC within the single-phonon and multiphonon schemes. The single-phonon rates vanish for transition energies larger than the greatest phonon frequency while the multiphonon rates cover a wide range of transition energies.

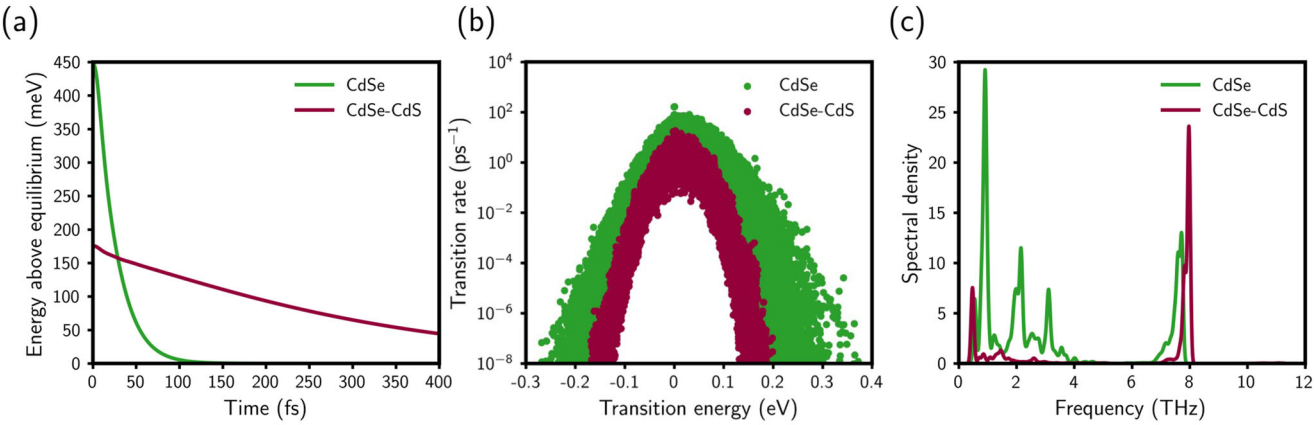

Fig. 4 Cooling in CdSe and CdSe-CdS core-shell NCs. a Hot exciton cooling simulated for a 3.9 nm CdSe NC and a 3.9 nm CdSe–3 monolayer CdS core-shell NC. Cooling in the core-shell NC occurs five times slower due to reduced EXPC. **b** Multiphonon transition rates calculated for the same CdSe and CdSe-CdS core-shell NCs, indicating that the rates for the core-shell NC are an order of magnitude smaller than that of the bare CdSe NC. **c** Calculated spectral densities for the same CdSe and CdSe-CdS core-shell NCs. The core-shell NC shows stronger EXPC to the CdSe optical modes (around 7.5 THz) than the bare CdSe NC. However, the bare CdSe NC has stronger coupling to lower- and mid-frequency modes, demonstrating that exciton coupling to a quasi-continuous frequency range of phonons is essential for efficient multiphonon relaxation.

previous expectations that only high-frequency optical modes would be responsible for cooling[15,28].

Figure 3a also demonstrates that smaller NCs relax more quickly to thermal equilibrium than larger NCs. Due to stronger quantum confinement, smaller NCs have more energy to dissipate during the cooling process. Smaller NCs also have larger excitonic gaps and a smaller number of phonon modes. However, smaller NCs have stronger EXPC than larger NCs[46], resulting in overall faster cooling timescales for smaller NCs.

Controlling the cooling timescales

The longer cooling timescales for larger CdSe NCs suggests that controlling the magnitude of EXPC may allow for tuning of the hot exciton cooling timescale. CdSe-CdS core-shell NCs have EXPC that is about five times smaller than that of bare cores due to suppression of exciton coupling to lower-frequency surface modes[46]. Figure 4a compares simulations of the cooling process for a 3.9 nm CdSe core and a 3.9 nm CdSe core with 3 monolayers of CdS shell. Because of the quasi-type II band alignment in CdSe-CdS core-shell NCs, the exciton hole is confined to the CdSe core while the electron somewhat delocalizes into the CdS shell[56]. This decreased quantum confinement leads to a smaller 1*P*-1*S* excitonic gap in core-shell NCs, so hot excitons have less energy to dissipate in core-shell NCs than in bare cores. However, cooling still takes about five times longer in the core-shell NC as a result of the weaker EXPC.

The multiphonon transition rates for both systems are shown in Fig. 4b, demonstrating that rates are one or more orders of magnitude smaller in the core-shell NC than in the bare core. For transitions with energies of 100 meV or less, the multiphonon relaxation rates range from $10^{-3} - 10^{2}$ ps^{-1} for the CdSe NC and from $10^{-4} - 10^{1}$ ps^{-1} for the CdSe-CdS core-shell NC.

We can further understand the role of EXPC in the cooling mechanism by examining the spectral densities, which describe the phonon densities of states weighted by the EXPC, of the core and core-shell NCs (Fig. 4c). The spectral density of the CdSe core shows significant EXPC to acoustic modes with frequencies of 4.0 THz or less, as well as optical modes between 7.5 and 8.0 THz[46,47]. The core-shell NC, however, has negligible EXPC at lower phonon frequencies, as the presence of the CdS shell prevents coupling to delocalized and surface-localized modes at those frequencies, but it has slightly stronger coupling to the CdSe optical modes. These results provide further evidence that both acoustic and optical modes play an essential role in the cooling process. Exciton coupling to phonons with a quasi-continuous frequency range allows for resonance conditions to be more easily satisfied; for every excitonic energy gap, a set of phonons with the corresponding energy is easily found. However, exciton coupling

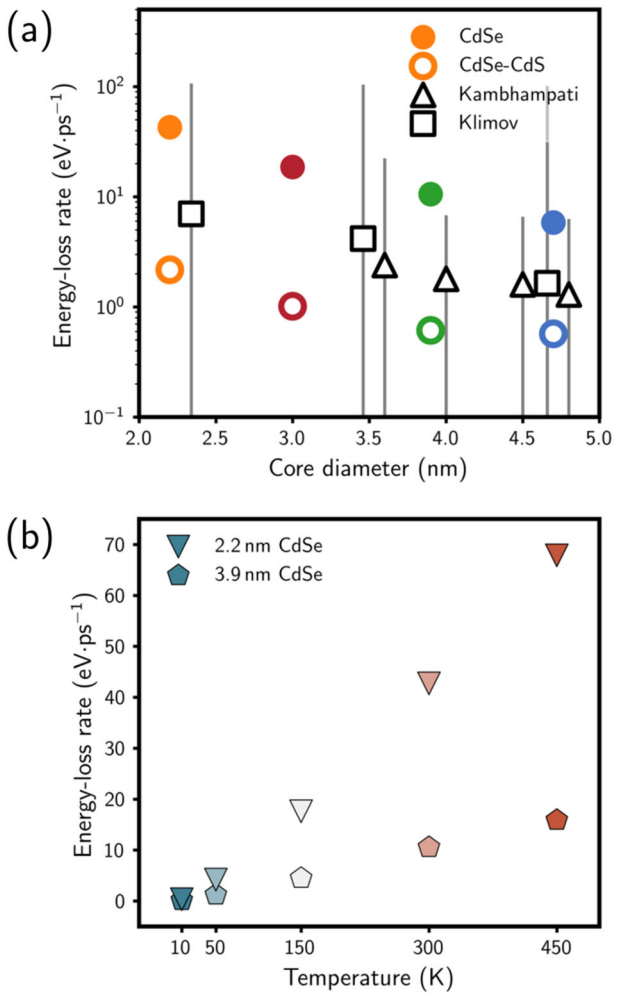

Fig. 5 Energy loss rates. a The energy loss rates calculated for CdSe and CdSe-CdS core-shell NCs. Core-shell structures all have 3 monolayers of shell. The black symbols correspond to measurements performed on CdSe NCs using transient absorption spectroscopy by Klimov et al.[26] and state-resolved pump-probe spectroscopy by Cooney et al.[30] Vertical grey lines correspond to experimental error bars. **b** The energy loss rates calculated for 2.2 nm CdSe and 3.9 nm CdSe NCs show a linear dependence on temperature with a stronger temperature-dependence for the 2.2 nm CdSe NC.

to phonons only within a narrow energy range restricts the set of phonons that would satisfy the necessary resonance conditions.

Energy loss rates

To allow for more meaningful comparison between our calculations and experimental measurements, we simulate changes in the absorption spectrum of a system initially excited to the 1*P* excitonic state as it relaxes to the 1*S* ground excitonic state. Assuming that the electric field, $\mathcal{E}$, is weak such that the population of the ground state remains approximately 1 and that the population of the excited state is proportional to $\mathcal{E}^2$, the change in absorption is given by

$$\begin{aligned}\Delta\sigma(\omega,t) &= \sigma_{\mathrm{exc}}(\omega) - \sigma_{\mathrm{gs}}(\omega,t)\\ &\propto \omega\mathcal{E}^2 \sum_n |\boldsymbol{\mu}_n|^2 p_n(t)\delta(\omega - E_n)\,,\end{aligned} \tag{7}$$

where $\boldsymbol{\mu}_n$ is the transition dipole moment from the ground state to excitonic state n and $p_n(t)$ is the population of excitonic state n at time t.

The change in absorption, $\Delta\sigma(\omega, t)$, shows a fast decay of the 1*P* excitonic peak and a slower rise of the 1*S* ground excitonic peak (Supplementary Fig. 3). The dynamics of the rise of the 1*S* peak reflect those of hot exciton cooling. For each system, the rise dynamics were fit to an exponential function, and the extracted timescale was divided by the energy difference between the 1*P* and 1*S* excitonic peaks to yield an energy loss rate. The calculated energy loss rates are illustrated in Fig. 5a along with those measured experimentally using transient absorption spectroscopy[26] and state-resolved pump-probe spectroscopy[30] on wurtzite CdSe NCs. In agreement with experiment, our simulations show faster energy loss rates for smaller CdSe NCs. Smaller NCs have larger excitonic gaps due to quantum confinement and a smaller number of phonon modes, but they have stronger EXPC than larger NCs. Similarly, core-shell NCs, which have significantly weaker EXPC to lower-frequency acoustic modes[46], show energy loss rates that are an order of magnitude slower than those of bare cores.

While Fig. 5a initially suggests that the calculated energy loss rates for CdSe NCs are larger than the measured values (but within the experimental error bars), those experiments use ~100 fs pulses that obscure the observation of dynamics between states with spectral overlap[57], like those measured here, and they measure NCs with very low photoluminescence quantum yields of around 1%, where carrier trapping may lead to dynamics that complicate the hot exciton cooling process. Two-dimensional electronic spectroscopy (ES) measurements, which are able to clearly resolve the features corresponding to excitonic relaxation, on 3.5 nm CdSe NCs show that hot exciton cooling from the higher-energy 1*S* excitonic peak to the ground excitonic peak occurs within ~30 fs[57], which is consistent with our findings. Furthermore, more recent two-dimensional ES experiments observe that cooling slows by an order of magnitude with the addition of a shell to a CdSe core[58], in agreement with our calculated results.

While changing the size and composition of NCs is one avenue for tuning the cooling timescale, changing the temperature is another. The energy loss rates for 2.2 nm CdSe and 3.9 nm CdSe NCs simulated at different temperatures are illustrated in Fig. 5b. For both NCs, the energy loss rates are ~0.1 eVps^{-1} at 10 K, and they monotonically increase with temperature, as expected for phonon-mediated processes. While both systems show a linear relationship between energy loss rate and temperature, the rate for the 2.2 nm NC shows a stronger dependence on temperature than that of the 3.9 nm NC. This steeper scaling with increasing temperature may be a result of the stronger quantum confinement in the 2.2 nm NC, which leads to larger energy gaps between excitonic states. Thus, multiphonon processes at larger transition energies are more important. As those transition rates are very sensitive to temperature (Supplementary Fig. 4), the overall cooling process in smaller NCs has a stronger temperature dependence. Interestingly, as shown in Supplementary Fig. 5, the single-phonon-mediated cooling process also depends on temperature, but the dynamics converge above a threshold temperature. The threshold temperature is ~300 K for the 2.2 nm CdSe NC, while it is ~50 K for the 3.9 nm CdSe. Again, this result may be due to the larger excitonic gaps in the smaller NC system. Note that our model given by Eq. (1) includes EXPC to lowest order in the phonon mode coordinates and ignores higher-order terms (Duschinsky rotations), which may influence the hot exciton cooling process at higher temperatures[59].

Mechanistic insight

Finally, we investigate the mechanism underlying this ultrafast hot exciton cooling process. We calculated the density of excitonic states for a 3.9 nm CdSe NC and scaled it by the time-dependent population, as illustrated in Fig. 6a. We see that cooling occurs *via* a cascade of relaxation events through the manifold of excitonic

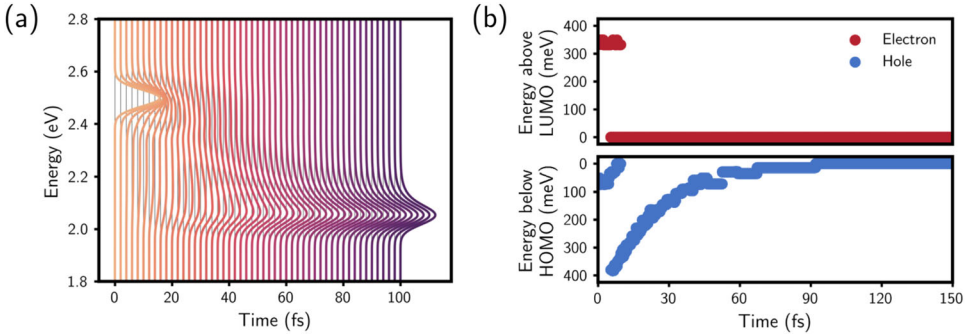

Fig. 6 Mechanistic details of hot exciton cooling in CdSe NCs. a The calculated density of excitonic states of a 3.9 nm CdSe NC scaled by the time-dependent population shows that hot exciton cooling occurs *via* a cascade of relaxation events. **b** Projection of exciton cooling dynamics for the same CdSe NC onto a single-particle, electron/hole picture shows consistency with the Auger cooling mechanism. Hole relaxation is followed by an Auger-like process that leads to electron relaxation to the band edge and hole re-excitation. The hole then relaxes again.

states, as opposed to being dominated by a single or a few higher-energy nonradiative transitions, as expected previously[15,16,28].

We wanted to understand the relationship between this multiphonon-mediated hot exciton cooling mechanism (Fig. 1c) and the Auger-assisted cooling mechanism (Fig. 1b), which was first proposed to explain the breaking of the phonon bottleneck[33]. The Auger relaxation event (i.e., the exchange of two electron-hole pairs, as illustrated in the second panel of Fig. 1b) is inherently included in the Bethe-Salpeter approach adopted here. Furthermore, in our excitonic picture, we see that the overall hot exciton cooling process occurs *via* a cascade of relaxation events. Thus, to make contact between our simulations and the Auger cooling mechanism, we projected our simulated exciton cooling dynamics for a 3.9 nm CdSe NC onto a single-particle picture of noninteracting electron-hole pair states (see SI for more details). As shown in Fig. 6b, we find that the Auger cooling mechanism emerges naturally from our excitonic dynamics. The hole quickly relaxes to the band edge *via* multiphonon emission followed by electron relaxation by ~400 meV that results in hole re-excitation, and then the hole once again relaxes to the band edge by multiphonon emission. This result indicates that *both* Coulomb-mediated electron-hole correlations, which are inherent in our formalism, *and* multiphonon-mediated excitonic transitions are required to circumvent the phonon bottleneck and lead to ultrafast timescales of hot exciton cooling. These mechanistic insights are consistent for core-shell NCs, as illustrated in Supplementary Fig. 6.

In conclusion, hot exciton cooling in confined semiconductor NCs involves rich physics, including electron-hole correlations, EXPC, and multiphonon-mediated nonradiative transitions—all of which are required to break the phonon bottleneck and enable fast relaxation of hot excitons to the band edge. We have developed an atomistic theory that describes multiphonon-mediated exciton dynamics in NCs of experimentally relevant sizes. Our approach yields cooling timescales of tens of femtoseconds, which are consistent with measurements of similar systems. These ultrafast timescales are enabled by a cascade of multiphonon-mediated transitions between excitonic states that are relatively close in energy. These nonradiative transitions are efficient, as the excitons are coupled to a large number of phonon modes in NCs that span a wide frequency range. The timescale of cooling is governed largely by the overall magnitude of EXPC, so that larger cores show slower relaxation, and core-shell NCs show relaxation that is slower by an order of magnitude.

Our approach provides fundamental insights to phonon-mediated exciton dynamics at the nanoscale, which differ significantly from those in molecular and bulk semiconductor systems. These simulations provide a unified, microscopic theory for hot exciton cooling in nanoscale systems that addresses longstanding questions regarding the timescales and mechanisms of this process and that provides design principles for NCs with tuned EXPC and cooling timescales. The framework presented here is sufficiently general that it can be used to study timescales and mechanisms of exciton dephasing and carrier trapping. Furthermore, it can be used to investigate dynamics in NCs of different dimensionalities, such as in nanorods and nanoplatelets, and materials, including III-V semiconductors, as long as EXPC is weak. Further elucidating the principles of phonon-mediated dynamics at the nanoscale is key to ultimately tuning these processes to realize novel phenomena in NC systems and NC-based applications with higher device efficiencies.

METHODS

As described in previous work[46], CdSe and CdSe-CdS core-shell structures were optimized *via* the LAMMPS molecular dynamics code[60] using Stillinger-Weber interatomic potentials[48]. The outermost atomic monolayer was then removed and the subsequent monolayer was replaced by potentials representing the passivation layer. Nanostructure configurations are given in Supplementary Tables I and II and illustrated in Supplementary Fig. 1.

Electronic structure calculations were performed using the semiempirical pseudopotential method[61–63] with pseudopotential parameters provided in Supplementary Table III. We used the filter diagonalization technique to solve for single-particle electron and hole states near the band edges and then used these as input to the Bethe-Salpeter equation, which was solved to obtain correlated electron-hole pair states[35]. The exciton-phonon couplings were calculated within this framework[46], and phonon modes and frequencies were obtained by diagonalizing the dynamical matrix computed using the same Stillinger-Weber interatomic potentials[48].

The correlation functions $\langle g_{n,m}(t)g_{m,n}(0)\rangle_{\mathrm{eq}}$ in Eq. (6) were evaluated within a harmonic approximation by sampling from a thermal distribution of bath coordinates and propagating classical trajectories. To facilitate convergence, we propagate and average trajectories to short times and then approximate the correlation functions as Gaussian functions. We also applied the standard quantum correction scheme to impose detailed balance[64]. Thus, the final transition rates are given by

$$\Gamma_{n\to m}(t)=\frac{4}{\hbar^2\left[1+e^{-\beta\hbar(\varepsilon_n-\varepsilon_m)}\right]}\int_0^t d\tau\cos((\varepsilon_n-\varepsilon_m)\tau/\hbar)\langle g_{n,m}(\tau)g_{m,n}(0)\rangle_{\mathrm{eq}}. \tag{8}$$

We computed rates for all transitions and used them to build a kinetic master equation (see Eq. (3)) and propagate phonon-mediated exciton dynamics. Further details for all methods are provided in the Supplementary Information.

DATA AVAILABILITY

All data that support the findings of this study and related codes are available from the corresponding author upon reasonable request.

CODE AVAILABILITY

All codes used to generate and analyze results supporting the finding of this study are available from the corresponding author upon reasonable request.

Received: 26 February 2023; Accepted: 28 July 2023;
Published online: 16 August 2023

REFERENCES

1. Lannoo, M., Delerue, C. & Allan, G. Theory of radiative and nonradiative transitions for semiconductor nanocrystals. *J. Lumin.* **70**, 170–184 (1996).
2. Klimov, V. I. Mechanisms for photogeneration and recombination of multiexcitons in semiconductor nanocrystals: Implications for lasing and solar energy conversion. *J. Phys. Chem. B* **110**, 16827–16845 (2006).
3. Sheik-Bahae, M. & Epstein, R. I. Optical refrigeration. *Nat. Photon.* **1**, 693–699 (2007).
4. Fomenko, V. & Nesbitt, D. J. Solution control of radiative and nonradiative lifetimes: A novel contribution to quantum dot blinking suppression. *Nano Lett.* **8**, 287–293 (2008).
5. Talapin, D. V., Lee, J. S., Kovalenko, M. V. & Shevchenko, E. V. Prospects of colloidal nanocrystals for electronic and optoelectronic applications. *Chem. Rev.* **110**, 389–458 (2010).
6. Hanifi, D. A. et al. Redefining near-unity luminescence in quantum dots with photothermal threshold quantum yield. *Science* **363**, 1199–1202 (2019).
7. Peterson, M. D. et al. The role of ligands in determining the exciton relaxation dynamics in semiconductor quantum dots. *Annu. Rev. Phys. Chem.* **65**, 317–339 (2014).
8. Melnychuk, C. & Guyot-Sionnest, P. Multicarrier dynamics in quantum dots. *Chem. Rev.* **121**, 2325–2372 (2021).
9. von der Linde, D. & Lambrich, R. Direct measurement of hot-electron relaxation by picosecond spectroscopy. *Phys. Rev. Lett.* **42**, 1090–1093 (1979).
10. Pugnet, M., Collet, J. & Cornet, A. Cooling of hot electron-hole plasmas in the presence of screened electron-phonon interactions. *Solid State Commun.* **38**, 531–536 (1981).
11. Prabhu, S. S., Vengurlekar, A. S., Roy, S. K. & Shah, J. Nonequilibrium dynamics of hot carriers and hot phonons in CdSe and GaAs. *Phys. Rev. B* **51**, 14233–14246 (1995).
12. Kambhampati, P. Hot exciton relaxation dynamics in semiconductor quantum dots: Radiationless transitions on the nanoscale. *J. Phys. Chem. C.* **115**, 22089–22109 (2011).
13. Knowles, K. E., McArthur, E. A. & Weiss, E. A. A multi-timescale map of radiative and nonradiative decay pathways for excitons in CdSe quantum dots. *ACS Nano* **5**, 2026–2035 (2011).
14. Jasrasaria, D., Weinberg, D., Philbin, J. P. & Rabani, E. Simulations of nonradiative processes in semiconductor nanocrystals. *J. Chem. Phys.* **157**, 020901 (2022).
15. Nozik, A. J. Spectroscopy and hot electron relaxation dynamics in semiconductor quantum wells and quantum dots. *Annu. Rev. Phys. Chem.* **52**, 193–231 (2001).
16. Inoshita, T. & Sakaki, H. Electron relaxation in a quantum dot: Significance of multiphonon processes. *Phys. Rev. B* **46**, 7260–7263 (1992).
17. Gfroerer, T. H. et al. Slow relaxation of excited states in strain-induced quantum dots. *Phys. Rev. B* **53**, 16474–16480 (1996).
18. Yu, H., Lycett, S., Roberts, C. & Murray, R. Time resolved study of self-assembled InAs quantum dots. *Appl. Phys. Lett.* **69**, 4087–4089 (1996).
19. Heitz, R. et al. Energy relaxation by multiphonon processes in InAs/GaAs quantum dots. *Phys. Rev. B* **56**, 10435–10445 (1997).
20. Guyot-Sionnest, P., Shim, M., Matranga, C. & Hines, M. Intraband relaxation in CdSe quantum dots. *Phys. Rev. B* **60**, R2181–R2184 (1999).
21. Sosnowski, T. S. et al. Rapid carrier relaxation in $In_{0.4}Ga_{0.6}As$/GaAs quantum dots characterized by differential transmission spectroscopy. *Phys. Rev. B* **57**, R9423–R9426 (1998).
22. Mukai, K. & Sugawara, M. Slow carrier relaxation among sublevels in annealed self-formed InGaAs/GaAs quantum dots. *Jpn. J. Appl. Phys.* **37**, 5451–5456 (1998).
23. Pandey, A. & Guyot-Sionnest, P. Slow electron cooling in colloidal quantum dots. *Science* **322**, 929–932 (2008).
24. Asahi, H. Self-organized quantum wires and dots in III–V semiconductors. *Adv. Mater.* **9**, 1019–1026 (1997).
25. Klimov, V. I. & McBranch, D. W. Femtosecond 1P-to-1S electron relaxation in strongly confined semiconductor nanocrystals. *Phys. Rev. Lett.* **80**, 4028–4031 (1998).
26. Klimov, V. I., McBranch, D. W., Leatherdale, C. A. & Bawendi, M. G. Electron and hole relaxation pathways in semiconductor quantum dots. *Phys. Rev. B* **60**, 13740–13749 (1999).
27. Klimov, V. I., Mikhailovsky, A. A., McBranch, D. W., Leatherdale, C. A. & Bawendi, M. G. Mechanisms for intraband energy relaxation in semiconductor quantum dots: The role of electron-hole interactions. *Phys. Rev. B* **61**, R13349–R13352 (2000).
28. Schaller, R. D. et al. Breaking the phonon bottleneck in semiconductor nanocrystals via multiphonon emission induced by intrinsic nonadiabatic interactions. *Phys. Rev. Lett.* **95**, 196401 (2005).
29. Harbold, J. M. et al. Time-resolved intraband relaxation of strongly confined electrons and holes in colloidal PbSe nanocrystals. *Phys. Rev. B* **72**, 195312 (2005).
30. Cooney, R. R. et al. Unified picture of electron and hole relaxation pathways in semiconductor quantum dots. *Phys. Rev. B* **75**, 245311 (2007).
31. Cooney, R. R., Sewall, S. L., Anderson, K. E. H., Dias, E. A. & Kambhampati, P. Breaking the phonon bottleneck for holes in semiconductor quantum dots. *Phys. Rev. Lett.* **98**, 177403 (2007).
32. Kharchenko, V. & Rosen, M. Auger relaxation processes in semiconductor nanocrystals and quantum wells. *J. Lumin.* **70**, 158–169 (1996).
33. Efros, A. L., Kharchenko, V. & Rosen, M. Breaking the phonon bottleneck in nanometer quantum dots: Role of Auger-like processes. *Solid State Commun.* **93**, 281–284 (1995).
34. Hendry, E. et al. Direct observation of electron-to-hole energy transfer in CdSe quantum dots. *Phys. Rev. Lett.* **96**, 057408 (2006).
35. Philbin, J. P. & Rabani, E. Electron-hole correlations govern Auger recombination in nanostructures. *Nano Lett.* **18**, 7889–7895 (2018).
36. Guyot-Sionnest, P., Wehrenberg, B. & Yu, D. Intraband relaxation in CdSe nanocrystals and the strong influence of the surface ligands. *J. Chem. Phys.* **123**, 074709 (2005).
37. Xu, S., Mikhailovsky, A. A., Hollingsworth, J. A. & Klimov, V. I. Hole intraband relaxation in strongly confined quantum dots: Revisiting the "phonon bottleneck" problem. *Phys. Rev. B* **65**, 045319 (2002).
38. Wang, L.-W., Califano, M., Zunger, A. & Franceschetti, A. Pseudopotential theory of Auger processes in CdSe quantum dots. *Phys. Rev. Lett.* **91**, 056404 (2003).
39. Kilina, S. V., Kilin, D. S. & Prezhdo, O. V. Breaking the phonon bottleneck in PbSe and CdSe quantum dots: Time-domain density functional theory of charge carrier relaxation. *ACS Nano* **3**, 93–99 (2009).
40. Prezhdo, O. V. Photoinduced dynamics in semiconductor quantum dots: Insights from time-domain ab initio studies. *Acc. Chem. Res.* **42**, 2005–2016 (2009).
41. Zeng, T. & He, Y. Ab initio modeling of phonon-assisted relaxation of electrons and excitons in semiconductor nanocrystals for multiexciton generation. *Phys. Rev. B* **103**, 1–15 (2021).
42. Li, X.-Q., Nakayama, H. & Arakawa, Y. Phonon bottleneck in quantum dots: Role of lifetime of the confined optical phonons. *Phys. Rev. B* **59**, 5069–5073 (1999).
43. Kilina, S. V., Craig, C. F., Kilin, D. S. & Prezhdo, O. V. Ab initio time-domain study of phonon-assisted relaxation of charge carriers in a PbSe quantum dot. *J. Phys. Chem. C.* **111**, 4871–4878 (2007).
44. Han, P. & Bester, G. Carrier relaxation in colloidal nanocrystals: Bridging large electronic energy gaps by low-energy vibrations. *Phys. Rev. B* **91**, 085305 (2015).
45. Pandey, A. & Guyot-Sionnest, P. Hot electron extraction from colloidal quantum dots. *J. Phys. Chem. Lett.* **1**, 45–47 (2010).
46. Jasrasaria, D. & Rabani, E. Interplay of surface and interior modes in exciton-phonon coupling at the nanoscale. *Nano Lett.* **21**, 8741–8748 (2021).
47. Jasrasaria, D. & Rabani, E. Correction to interplay of surface and interior modes in exciton–phonon coupling at the nanoscale. *Nano Lett.* **22**, 8033–8034 (2022).
48. Zhou, X. W. et al. Stillinger-Weber potential for the II-VI elements Zn-Cd-Hg-S-Se-Te. *Phys. Rev. B* **88**, 085309 (2013).
49. Sewall, S. L., Cooney, R. R., Anderson, K. E., Dias, E. A. & Kambhampati, P. State-to-state exciton dynamics in semiconductor quantum dots. *Phys. Rev. B* **74**, 235328 (2006).
50. Redfield, A. G. On the theory of relaxation processes. *IBM J. Res. Dev.* **1**, 19–31 (1957).
51. Nitzan, A. & O. U. Press. *Chemical Dynamics in Condensed Phases: Relaxation, Transfer and Reactions in Condensed Molecular Systems*, Oxford Graduate Texts. OUP Oxford (2006), ISBN 9780198529798.
52. Zimanyi, E. N. & Silbey, R. J. Theoretical description of quantum effects in multichromophoric aggregates. *Philos. Trans. R. Soc. A* **370**, 3620–3637 (2012).
53. Xu, D. & Cao, J. Non-canonical distribution and non-equilibrium transport beyond weak system-bath coupling regime: A polaron transformation approach. *Front. Phys.* **11**, 110308 (2016).
54. Franchini, C., Reticcioli, M., Setvin, M. & Diebold, U. Polarons in materials. *Nat. Rev. Mater.* **6**, 560–586 (2021).

55. Englman, R. & Jortner, J. The energy gap law for radiationless transitions in large molecules. *Mol. Phys.* **18**, 145–164 (1970).
56. Eshet, H., Grünwald, M. & Rabani, E. The electronic structure of CdSe/CdS core/shell seeded nanorods: Type-I or quasi-type-II? *Nano Lett.* **13**, 5880–5885 (2013).
57. Griffin, G. B. et al. Two-dimensional electronic spectroscopy of CdSe nanoparticles at very low pulse power. *J. Chem. Phys.* **138**, 014705 (2013).
58. Brosseau, P. J. et al. New ultrafast hole relaxation channels in quantum dots revealed by two-dimensional electronic spectroscopy. *Commun. Phys.* **6**, 48 (2023).
59. Lin, K. et al. Theory of photoluminescence spectral line shapes of semiconductor nanocrystals. https://doi.org/10.1021/acs.jpclett.3c01630 (2022).
60. Plimpton, S. Fast parallel algorithms for short-range molecular dynamics. *J. Comput. Phys.* **117**, 1–19 (1995).
61. Wang, L. W. & Zunger, A. Electronic structure pseudopotential calculations of large (~1000 atoms) Si quantum dots. *J. Phys. Chem.* **98**, 2158–2165 (1994).
62. Wang, L.-W. & Zunger, A. Pseudopotential calculations of nanoscale CdSe quantum dots. *Phys. Rev. B* **53**, 9579–9582 (1996).
63. Rabani, E., Hetenyi, B., Berne, B. J. & Brus, L. E. Electronic properties of CdSe nanocrystals in the absence and presence of a dielectric medium. *J. Chem. Phys.* **110**, 5355–5369 (1999).
64. Egorov, S. & Skinner, J. Semiclassical approximations to quantum time correlation functions. *Chem. Phys. Lett.* **293**, 469–476 (1998).

ACKNOWLEDGEMENTS

E.R. acknowledges support from the U.S. Department of Energy, Office of Science, Office of Advanced Scientific Computing Research, Scientific Discovery through Advanced Computing (SciDAC) program under Award No. DE-SC0022088. Methods used in this work were provided by the Center for Computational Study of Excited State Phenomena in Energy Materials (C2SEPEM), which is funded by the U.S. Department of Energy, Office of Science, Basic Energy Sciences, Materials Sciences and Engineering Division, via Contract No. DE-AC02-05CH11231, as part of the Computational Materials Sciences Program. D.J. acknowledges the support of the Computational Science Graduate Fellowship from the U.S. Department of Energy under Grant No. DE-SC0019323.

AUTHOR CONTRIBUTIONS

D.J. and E.R. conceived and designed the research. D.J. developed the code and performed all simulations under the supervision of E.R. D.J. and E.R. analyzed and interpreted results. D.J. and E.R. contributed to writing and preparing the manuscript.

COMPETING INTERESTS

The authors declare no competing interests.

ADDITIONAL INFORMATION

Supplementary information The online version contains supplementary material available at https://doi.org/10.1038/s41524-023-01102-8.

Correspondence and requests for materials should be addressed to Dipti Jasrasaria or Eran Rabani.

Reprints and permission information is available at http://www.nature.com/reprints

Publisher's note Springer Nature remains neutral with regard to jurisdictional claims in published maps and institutional affiliations.